




Symmetry determined topology from flux dimerization

Gang Jiang ¹, Z. Y. Chen,¹ S. J. Yue,¹ W. B. Rui,^{2,3} Xiao-Ming Zhu,⁴ Shengyuan A. Yang ⁵ and Y. X. Zhao ^{2,3,*}¹National Laboratory of Solid State Microstructures and Department of Physics, Nanjing University, Nanjing 210093, China²Department of Physics and HKU-UCAS Joint Institute for Theoretical and Computational Physics at Hong Kong, The University of Hong Kong, Pokfulam Road, Hong Kong, China³HK Institute of Quantum Science & Technology, The University of Hong Kong, Pokfulam Road, Hong Kong, China⁴Hangzhou Yingshi Technology Co., Ltd, 153 Lianchuang Street, Yuhang District, Hangzhou 310000, China⁵Research Laboratory for Quantum Materials, IAPME, University of Macau, Macau, China

(Received 4 December 2023; accepted 12 March 2024; published 27 March 2024)

In the field of symmetry-protected topological phases, a common wisdom is that the symmetries may fix the nontrivial topological classifications, but they alone cannot determine whether a system is topologically nontrivial. Here, we show that this is no longer true in cases where symmetries are projectively represented. Particularly, the Zak phase, a topological invariant of a one-dimensional system, can be entirely determined by the projective symmetry algebra (PSA). To demonstrate this remarkable effect, we propose a minimal model, termed the flux Su-Schrieffer-Heeger (f-SSH) model, where the bond dimerization in the original SSH model is replaced by a flux dimerization. We present experimental realization of the f-SSH model in an electric-circuit array, and our predictions are directly confirmed by electric measurement. Our work refreshes the understanding of the relationship between symmetry and topology, opens up avenues for exploring novel PSA determined topological phases, and suggests flux dimerization as an approach for designing topological crystals.

DOI: [10.1103/PhysRevB.109.115155](https://doi.org/10.1103/PhysRevB.109.115155)

I. INTRODUCTION

Symmetry-protected topological phases have been a focus of physics research in the past two decades [1–7]. In general, the action of symmetries on a physical system is described by their representations. Such actions impose constraints on the physical state and decide its topological classification, i.e., what are possible topologically distinct phases allowed by the symmetries. Nevertheless, knowing the symmetries and their representations alone does not automatically tell us which phase (trivial or nontrivial) the system belongs to, which is a common wisdom well known in the field [1–7].

To illustrate this point, recall the famous Su-Schrieffer-Heeger (SSH) model [8] (see Fig. 1). Topological classification of the SSH model can result from several choices of symmetries. Let us consider the spacetime inversion PT being the protecting symmetry, which leads to a \mathbb{Z}_2 classification, with the nontrivial and trivial phases characterized by the Zak phase $\gamma = \pi$ and 0, respectively [9,10]. In the SSH chain, the two phases correspond to the two bond dimerization patterns shown in Fig. 1. Namely, in the unit cell (compatible with boundary condition), the nontrivial (trivial) phase has the intercell bond stronger (weaker) than the intracell bond. One can see that the symmetry determines the \mathbb{Z}_2 classification, but it cannot determine which phase an SSH chain belongs to. Indeed, the two phases in Figs. 1(a) and 1(b) correspond to the same symmetry representation, satisfying the same

group relations

$$(PT)^2 = 1, \quad (PT)L(PT) = L^{-1}, \quad (1)$$

where L is the unit translation along the chain [11].

In the presence of gauge fluxes, ordinary symmetry relations are extended into projective symmetry algebras (PSAs) [12–18]. That is, the successive action of two crystal symmetry operators S_1 and S_2 may be modified by an additional phase factor: $\rho(S_1)\rho(S_2) = \Omega(S_1, S_2)\rho(S_1S_2)$, where $\rho(S)$ denotes the projective representation of S . In general, the phase factor $\Omega(S_1, S_2)$ is valued in $U(1)$ [12], but under time-reversal symmetry T , it will be restricted to $\mathbb{Z}_2 = \{\pm 1\}$ [15]. Recently, it was realized that PSAs could enable a novel class of symmetry-protected topological phases with much richer properties compared to conventional ones. Examples include the Mobius insulator [14,19,20], real topological charges [21,22], realization of spinful topological phases by spinless systems [23–27], and k -space nonsymmorphic symmetry protected topological phases such as the Klein-bottle insulator [28–36].

In this work, we discover that the aforementioned common wisdom is violated for PSA enabled topological phases; namely, knowing certain projective symmetry representations alone is sufficient to completely determine the topological phase. We demonstrate this remarkable phenomenon in a minimal model, named the flux Su-Schrieffer-Heeger (f-SSH) model, where the bond dimerization of the original SSH model is replaced by a “flux dimerization.” We show that the Zak phase of the f-SSH model is an invariant of PSA; i.e., it is solely determined by the symmetries’ projective representations. Furthermore, distinct from conventional topological

*yuxinphy@hku.hk

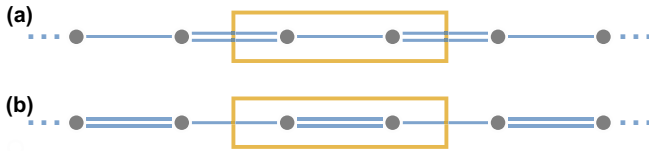


FIG. 1. Two phases of the standard SSH model. (a) The topological phase with intercell bond stronger than the intracell bond. (b) The trivial phase with intercell bond weaker than the intracell bond.

phases, where different bands are allowed to have different Zak phases, the Zak phases enforced by PSA must be the same for all the bands. Our theory is experimentally verified in a topological electric circuit realizing the f-SSH model, where the topological boundary modes, the manifestation of the PSA dictated Zak phase, are confirmed by direct electric measurement. Our work reveals a fascinating connection between symmetry and topology in PSA enabled topological phases, and provides a new strategy to explore topological phases via designed PSAs and the method of flux dimerization.

II. THE f-SSH MODEL

Our f-SSH model is shown in Fig. 2(a). In this model, a unit cell has four sites. All hoppings between nearest neighbors have the same magnitude, but their signs can be positive or negative, denoted by blue and red colors in Fig. 2(a). Going around a plaquette, the accumulation of hopping signs

correspond to a gauge flux of 0 or π . The f-SSH model has an alternating distribution of 0 and π fluxes.

Similar to the original SSH model, this model also preserves P , T , and L symmetries. However, the flux dimerization modifies the representation of these symmetries and their PSA in a fundamental way. Consider the inversion operation. With the inversion center at the center of a π -flux plaquette, direct inversion transforms the chain from Fig. 2(a) to Fig. 2(b). One observes that although the flux distribution is preserved, the color of the bonds, i.e., the gauge connection configuration, is not. To recover the original configuration in Fig. 2(a), an additional gauge transformation G is required. For our current case, G is illustrated in Fig. 2(c), which involves a sign (π -phase) change at some of the local basis states. It follows that the representation of inversion in the f-SSH model is a combined operation:

$$\mathbf{P} = GP. \quad (2)$$

It is this operator \mathbf{P} that commutes with the Hamiltonian.

Importantly, G does not commute with P and L . Instead, we have $PGP^{-1} = -G$ and $LGL^{-1} = -G$, as reflected in Fig. 2(c) by noticing that both P and L inverse the sign of G . Then, one immediately observes that the relations in Eq. (1) satisfied by the ordinary representation are now modified into a PSA, with

$$(\mathbf{PT})^2 = -1 \quad (3)$$

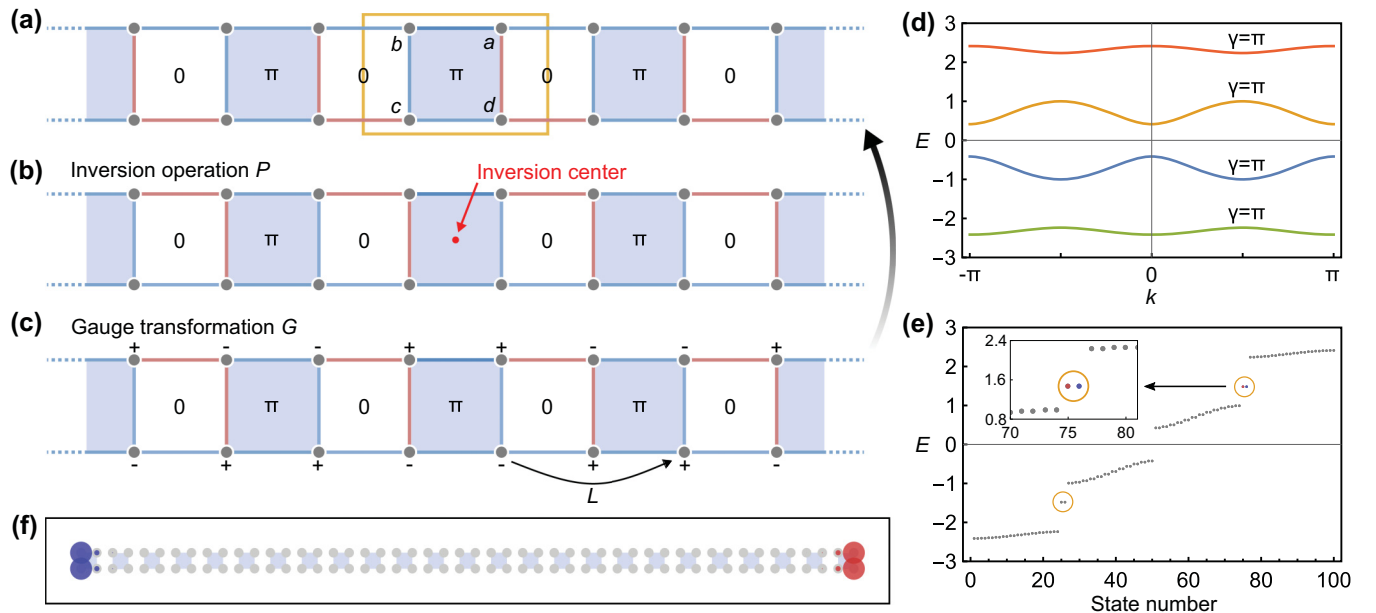


FIG. 2. (a) Illustration of the f-SSH model. A unit cell (marked by the yellow box) contains four sites, labeled by a , b , c , and d . All hopping amplitudes have the same magnitude but may have different signs. The negative and positive ones are marked in red and blue, respectively. These signs result in a flux distribution as indicated in the figure. (b) Direct inversion operation with respect to the inversion center (red dot) does not preserve the gauge configuration; i.e., the colors of the bonds are changed from those in (a). (c) An additional gauge transformation G is required to recover the original configuration in (a). Here, the plus and minus signs indicate the phase change of the local basis at respective sites. One observes that this G does not commute with L and P , as both L and P exchange \pm signs. (d) Band structure of the f-SSH model. All bands have Zak phase π as determined by the PSA. (e) Energy spectrum for the model with a length of 25 unit cells. The in-gap states are surrounded by orange circles. (f) Spatial distribution of the two in-gap states in the third gap as indicated in the insert of (e). The two states are distributed at two ends, and they represent the topological end states corresponding to the nontrivial Zak phase.

and

$$(\mathbf{PT})L(\mathbf{PT})^{-1} = -L^{-1}. \quad (4)$$

The minus signs in the two identities are *invariants* of the PSA, as shown in Appendix A. Here, we note that only the combined symmetry \mathbf{PT} is required to be preserved, while both \mathbf{P} and T can be broken.

More importantly, the PSA in Eqs. (3) and (4) dictates the value of the Zak phase. To see this, note that in k space, L is represented by e^{ik} (taking the lattice constant to be unit); then Eq. (4) indicates that \mathbf{PT} must send k to $k + \pi$. Consider a single band $|\psi(k)\rangle$ with periodicity $|\psi(k)\rangle = |\psi(k + 2\pi)\rangle$. Then the \mathbf{PT} operator acts on the band as

$$U_{PT}|\psi(k)\rangle^* = e^{i\phi(k)}|\psi(k + \pi)\rangle, \quad (5)$$

where we expressed $\mathbf{PT} = U_{PT}K$ with U_{PT} a unitary operator and K the complex conjugation. This equation means that \mathbf{PT} maps $|\psi(k)\rangle$ to $|\psi(k + \pi)\rangle$ up to a phase factor $e^{i\phi(k)}$.

From Eq. (3), we have $U_{PT}U_{PT}^* = -1$, which leads to

$$e^{i\phi(k+\pi)-i\phi(k)} = -1. \quad (6)$$

Hence, the PSA establishes a connection between states at k and $k + \pi$.

Using Eqs. (5) and (6), one can readily evaluate the Zak phase [9],

$$\gamma = \oint dk \langle \psi(k) | i\partial_k | \psi(k) \rangle, \quad (7)$$

by dividing the integration domain into two parts, $[-\pi, 0]$ and $[0, \pi]$, and relating the two by \mathbf{PT} (see Appendix B). For a single band, one finds that the Zak phase is guaranteed to be $\gamma = \pi$. It must be pointed out that the above analysis is completely general: We never used any details of the single band except the PSA in Eqs. (3) and (4) that the model satisfies. In other words, if an isolated band appears in a system with the PSA, its Zak phase is determined to be nontrivial by the PSA.

When will the Zak phase be zero? From the above discussion, this must occur in a configuration with a different PSA. For the f-SSH model, this corresponds to the unit cell choice with inversion center at zero-flux plaquette. One can easily check that in this case, although Eq. (4) remains the same, Eq. (5) is changed to $(\mathbf{PT})^2 = +1$, which then dictates that $\gamma = 0$.

Thus, the two topological phases of the flux SSH model directly correspond to two distinct PSAs, with $(\mathbf{PT})^2 = \alpha \in \{\pm 1\}$, such that the Zak phase can be expressed as

$$\gamma = i \ln \alpha \quad \text{mod } 2\pi. \quad (8)$$

This is in contrast to conventional cases, where symmetries [as in Eq. (1)] cannot determine the topological phase.

Our claims above are confirmed by a direct calculation of the model (see Appendix C). Figures 2(d)–2(f) show the nontrivial case with PSA in Eqs. (5) and (6). The calculated band structure is plotted in Fig. 2(d), and we verified that each band here has a π Zak phase. This is another salient feature distinct from conventional systems, where different bands are not guaranteed to have the same Zak phase.

A π Zak phase requires the presence of 0D topological modes at the end of the 1D chain. In our model, this occurs for the first and the third bulk band gaps (the second gap is trivial since the Zak phases for the two bands below add up to zero). Such topological end modes are confirmed in Fig. 2(e), by our calculation of a chain with a finite length. The profiles of the two in-gap states in the third gap are plotted in Fig. 2(f).

III. EXPERIMENTAL DEMONSTRATION

The proposed f-SSH model constitutes a minimal model for the PSA determined topology. Below, we present experimental realization of this model in an electric-circuit array, which directly verifies our theory. Some universal methods to implement negative hopping amplitudes in a tight-binding model can be found in Ref. [21].

Electric circuits are governed by Kirchoff's law. In the frequency domain, it assumes the general form of $I_i(\omega) = \sum_j J_{ij}(\omega)V_j(\omega)$, where $I_i(\omega)$ and $V_i(\omega)$ are the electric current and voltage at node i , $J_{ij}(\omega)$ is the admittance between nodes i and j , and the summation is over all adjacent nodes. It follows that the behavior of a circuit is characterized by its $J(\omega)$ matrix, also known as the circuit Laplacian, and the task is to design a circuit whose $J(\omega)$ matrix can simulate the f-SSH model.

The design is straightforward, thanks to the characters of capacitors and inductors which naturally exhibit a phase difference in their responses [37–39]. As shown in Fig. 3(a), one just needs to use capacitor (C_1) for the blue bond and inductor (L_1) for the red bond. Then a unit cell contains four capacitors and two inductors (and four nodes). The additional inductors and capacitors (with values L_1 and C_2) at the top and bottom in Fig. 3(a) are used to facilitate measurement. They are not essential to PSA and topology.

For this simple circuit array, one readily derives that

$$J(\omega, k) = i\omega C_1 H(\omega, k), \quad (9)$$

and at driving frequency $\omega = \omega_0 \equiv 1/\sqrt{L_1 C_1}$,

$$H(\omega_0, k) = \mathcal{H}_{\text{fSSH}}(k) - \lambda \mathbb{1}, \quad (10)$$

where $\mathcal{H}_{\text{fSSH}}$ is just the f-SSH model put in dimensionless form (see Appendix E), and $\lambda = C_2/C_1$ is a constant shift that can be utilized to probe the topological end mode.

The measurement is on the impedance response $Z_{ab}(\omega)$ between two nodes a and b , which can be expressed as

$$Z_{ab}(\omega) = \frac{V_a - V_b}{I_{ab}} = \sum_n \frac{|\psi_{n,a} - \psi_{n,b}|^2}{j_n(\omega)}, \quad (11)$$

where j_n and $\{\psi_{n,i}\}$ are the n th eigenvalue and eigenmode of $J(\omega)$. In $Z_{ab}(\omega)$, the mode with j_n close to zero (called the zero-admittance mode) will dominate the response. For any target mode, we can utilize the λ term in Eq. (10) (by tuning C_2) to shift its eigenvalue to zero. Here, we focus on the topological end mode corresponding to the one in the third gap of $\mathcal{H}_{\text{fSSH}}$ in Fig. 1(e), which has a value of ~ 1.48 , so we choose $\lambda = 1.48$ in our design. This makes the topological end mode the zero-admittance mode at frequency $\omega = \omega_0$. In Fig. 3(c), we show the simulated $J(\omega)$ spectrum of our designed circuit, which confirms this point.

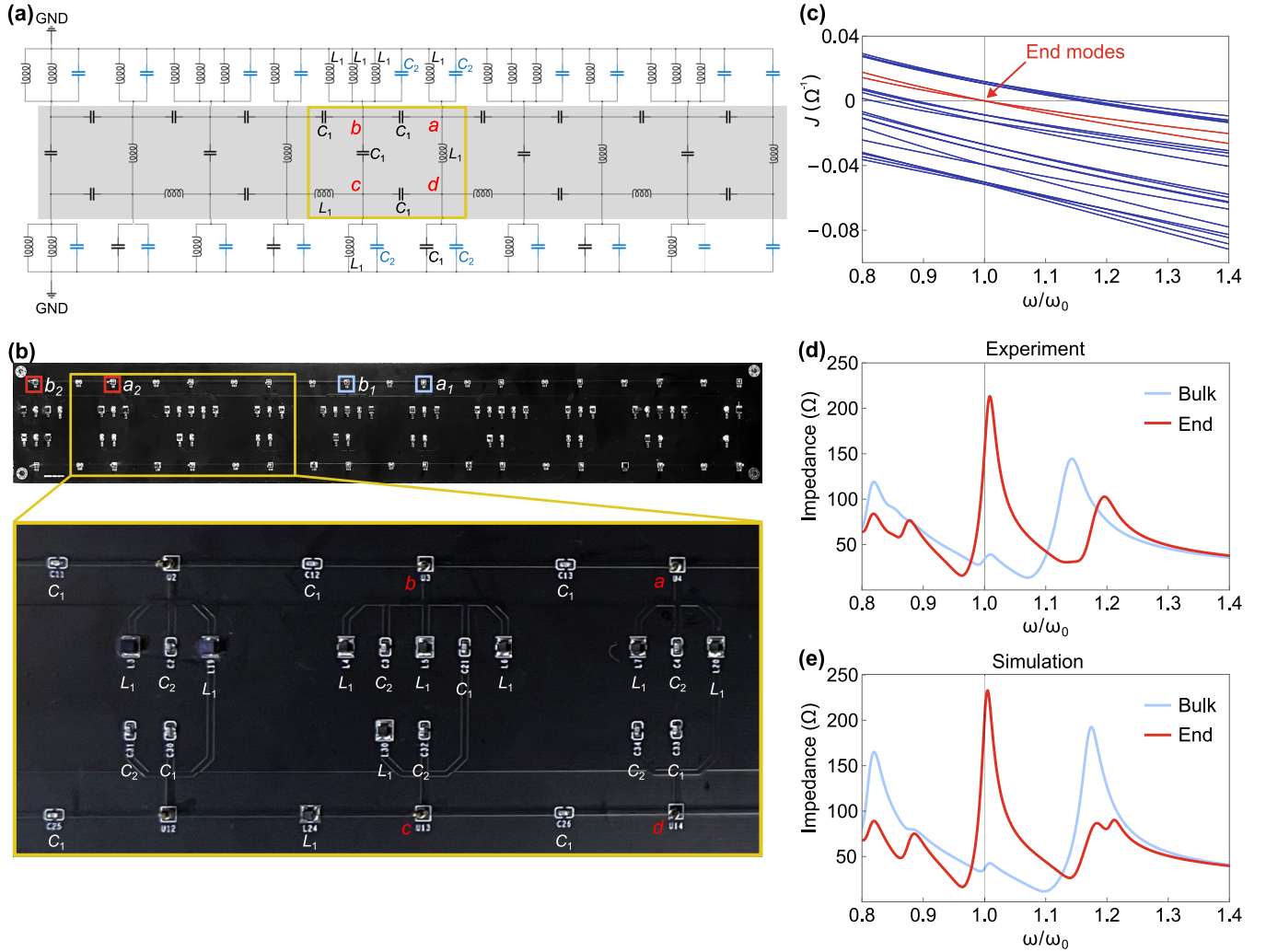


FIG. 3. (a) Circuit diagram for the f-SSH model with five unit cells. The shadowed area faithfully simulates the f-SSH model. Each inductor (capacitor) corresponds to a negative (positive) hopping amplitude. A unit cell is indicated by the yellow rectangular. The remaining part is designed to tune the reference voltage of the electric circuit. (b) Photograph of our fabricated circuit board. (c) Theoretical spectrum of the circuit Laplacian as a function of the driving frequency. All frequency scales are normalized to the resonance frequency ω_0 . Two isolated modes crossing the gap, which correspond to zero-energy eigenvalues of the circuit Laplacian at $\omega = \omega_0$, are marked in red. They correspond to the two topological end modes. (d), (e) Experimental and simulated impedance responses versus normalized frequency. The end (bulk) impedance is measured between a_2 (a_1) and b_2 (a_2) in (b). The curve at the end (in the bulk) is marked in red (blue). The experimental curves well agree with the simulation curves, confirming the topological end states of the f-SSH model.

Experimentally, we fabricate the designed circuit on a printed circuit board, as shown in the photo in Fig. 3(b). It has a length of five unit cells, not long but sufficient to discern the topological end modes. We perform impedance measurement on two pairs of nodes. The first pair a_1 and b_1 are in the bulk (the middle cell), and the second pair a_2 and b_2 are at the end (the first cell), as indicated in Fig. 3(b). From the above analysis, one expects that the topological end mode of the f-SSH model should manifest as a peak at $\omega = \omega_0$ for measurement at a_2 and b_2 , and this peak will disappear for measurement at a_1 and b_1 . This is confirmed by the measured results in Fig. 3(d). The experimental curves also agree very well with results from numerical simulations of the circuit [see Fig. 3(e)]. These results confirm the PSA enforced topology in this topological circuit.

IV. DISCUSSION

We have discovered an extraordinary phenomenon beyond the common wisdom regarding topological phases; i.e., a particular projective algebraic structure of symmetries can completely determine certain topological invariants. We propose a simple model, the f-SSH model, which demonstrates the phenomenon. Remarkably, every isolated band is enforced by PSA to have a nontrivial Zak phase. We also provide experimental proof of this phenomenon using a designed electric circuit array. Considering the rich crystal symmetries, we expect that there will be an abundance of such intriguing effects to be discovered for PSA enabled topological phases. Moreover, our proposed flux dimerization may serve as an effective design strategy to realize novel PSA determined topological phases, applying to a wide range of

physical systems besides electric circuits, such as cold atoms [40,41], phononic/photonic crystals [42–45], and mechanical networks [46,47].

ACKNOWLEDGMENTS

The authors thank D. L. Deng for valuable discussions. This work is supported by the National Natural Science Foundation of China (Grants No. 12161160315 and No. 12174181), the Basic Research Program of Jiangsu Province (Grant No. BK20211506), and a UM Start-up Grant (No. SRG2023-00057-IAPME).

APPENDIX A: GAUGE INVARIANCE OF PSA

One may modify \mathbf{PT} by an arbitrary phase $e^{i\theta}$, as $\mathbf{PT} \mapsto e^{i\theta}\mathbf{PT}$. One finds that

$$\begin{aligned} (e^{i\theta}\mathbf{PT})^2 &= e^{i\theta}\mathbf{PT}e^{i\theta}\mathbf{PT} \\ &= e^{i\theta}e^{-i\theta}(\mathbf{PT})^2 = (\mathbf{PT})^2. \end{aligned} \quad (\text{A1})$$

In the second equality, we have used the fact that \mathbf{PT} is antiunitary, and therefore a complex number is conjugated after commuting with \mathbf{PT} . Hence, we see $(\mathbf{PT})^2 = \alpha$ is gauge invariant. It is known as a cohomology invariant for the PSA. Similarly, one can verify the invariance of Eq. (4) in the main text under $\mathbf{PT} \mapsto e^{i\theta}\mathbf{PT}$ and $L \mapsto e^{i\theta}L$.

APPENDIX B: DERIVATION OF THE ENFORCED ZAK PHASE

The integrand in Eq. (7) in the main text is known as the Berry connection $\mathcal{A}(k)$. From Eq. (5) in the main text, we find that

$$|\psi(k + \pi)\rangle = e^{-i\phi(k)}U_{PT}|\psi(k)\rangle^*. \quad (\text{B1})$$

Substituting this into the Berry connection expression at $k + \pi$, we obtain

$$\mathcal{A}(k + \pi) = -\mathcal{A}(k) + \partial_k\phi(k). \quad (\text{B2})$$

Hence, the Zak phase can be expressed as

$$\gamma = \int_0^\pi dk [\mathcal{A}(k) + \mathcal{A}(k + \pi)] = \phi(\pi) - \phi(0). \quad (\text{B3})$$

Then, using Eq. (6) in the main text, we find that $\gamma = \pi$.

In addition, following similar derivation, one finds that for PSA with $(\mathbf{PT})^2 = \alpha \in \{\pm 1\}$ and $(\mathbf{PT})L(\mathbf{PT})^{-1} = -L^{-1}$, we must have

$$\gamma = i \ln \alpha \pmod{2\pi}, \quad (\text{B4})$$

which is Eq. (8) in the main text.

APPENDIX C: FLUX SSH MODEL

Our proposed flux SSH model is a minimal model that realizes the PSA in Eqs. (3) and (4) in the main text. According

to Fig. 2(a), the explicit form of the model in real space can be written as

$$\begin{aligned} H &= t \sum_i (c_{i,a}^\dagger c_{i,b} + c_{i,b}^\dagger c_{i,c} + c_{i,c}^\dagger c_{i,d} - c_{i,d}^\dagger c_{i,a}) \\ &\quad + t \sum_i (c_{i+1,b}^\dagger c_{i,a} - c_{i+1,c}^\dagger c_{i,d}) + \text{H.c.}, \end{aligned} \quad (\text{C1})$$

where the hopping parameter t is taken to be real positive, i labels the unit cell, the first term is intracell hopping, and the second term is intercell hopping. For the minimal model, we include the nearest-neighbor hopping. One can certainly add more complicated terms, such as far-neighbor hoppings, but as long as they respect the PSA, the topological character of the system must remain unchanged.

Transforming to k space, the flux SSH model takes the form of

$$\mathcal{H}_{\text{fSSH}} = \begin{bmatrix} 0 & 1 + e^{ik} & 0 & -1 \\ 1 + e^{-ik} & 0 & 1 & 0 \\ 0 & 1 & 0 & 1 - e^{-ik} \\ -1 & 0 & 1 - e^{ik} & 0 \end{bmatrix}, \quad (\text{C2})$$

where we put it in dimensionless form (in unit of t). Its band structure consists of four bands with

$$E(k) = \pm\sqrt{3 \pm 2\sqrt{1 + \cos^2 k}}, \quad (\text{C3})$$

which has been plotted in Fig. 2(d). Direct calculation shows that every band here carries a π Zak phase, as we predicted based on PSA. The topological end modes for a flux SSH chain with 25 unit cells have been confirmed by the results in Figs. 2(e) and 2(f).

In connection with the original SSH model, we also provide the following intuitive picture. In the flux SSH model, consider the coupling between two neighboring sites along the chain, e.g., between sites a and b . One can readily identify two leading interaction paths; one is direct hopping between the two, and the other is to go around three edges of a plaquette. Then, the effective hopping amplitude is the superposition of two paths. Clearly, the coupling is enhanced for 0-flux plaquettes and reduced for π -flux plaquettes. As a result, one can imagine that the effective hopping amplitudes form a dimerization pattern similar to the original SSH model. This offers an intuitive understanding of the result.

APPENDIX D: THE SPACETIME INVERSION OPERATOR

For the flux SSH model with $\mathcal{H}_{\text{fSSH}}(k)$ in Eq. (C2), the unitary matrix associated to \mathbf{PT} is given by

$$U_{PT} = \begin{bmatrix} 0 & 0 & -1 & 0 \\ 0 & 0 & 0 & -1 \\ 1 & 0 & 0 & 0 \\ 0 & 1 & 0 & 0 \end{bmatrix}, \quad (\text{D1})$$

which satisfies

$$U_{PT}U_{PT}^* = -1. \quad (\text{D2})$$

It is straightforward to verify that

$$U_{PT} \mathcal{H}_{\text{SSH}}^*(k) U_{PT}^\dagger = \mathcal{H}_{\text{SSH}}(k + \pi); \quad (\text{D3})$$

i.e., PT translates k by π .

APPENDIX E: J MATRIX FOR THE FLUX SSH CIRCUIT

By Kirchhoff's law, our designed circuit has its circuit Laplacian $J(\omega, k) = i\omega C_1 H(\omega, k)$, where

$$H(\omega, k) = \begin{bmatrix} 2\eta - \lambda & 1 + e^{ik} & 0 & -\zeta \\ 1 + e^{-ik} & 3\eta - \lambda & 1 & 0 \\ 0 & 1 & 2\eta - \lambda & 1 - \zeta e^{-ik} \\ -\zeta & 0 & 1 - \zeta e^{ik} & 2\eta - \lambda \end{bmatrix},$$

where $\eta = (L_1 C_1)^{-1}/\omega^2 - 1$, $\zeta = (L_1 C_1)^{-1}/\omega^2$, and $\lambda = C_2/C_1$. When we tune the driving frequency ω to the LC resonance frequency $\omega_0 = 1/\sqrt{L_1 C_1}$, we have $\eta = 0$ and $\zeta = 1$. Compared with the flux SSH model in Eq. (C2), we

immediately notice that

$$H(\omega_0, k) = \mathcal{H}_{\text{SSH}}(k) - \lambda 1. \quad (\text{E1})$$

Therefore, the designed circuit constitutes a realization of our proposed flux SSH model.

APPENDIX F: EXPERIMENTAL DETAILS

In the designed circuit, we choose $C_1 = 1$ nF, $L_1 = 5.6$ μ H, so the resonant frequency is 2.1268 MHz. Ideally, a single capacitor with capacitance 1.48 nF can be chosen to realize the desired C_2 , but in practice, it is difficult to find proper capacitors with this exact value. Therefore, we use two capacitors whose capacitances are $C_{2a} = 1$ nF and $C_{2b} = 0.47$ nF in parallel to realize C_2 . In this way, the capacitance C_2 achieved is 1.47 nF, slightly lower than the ideal value.

In the electric circuit that we fabricated, the part number of C_1 and C_{2a} is GRM1885C1H102FA01D, the part number of L_1 is SLF10145T-5R6M3R2-PF, and the part number of C_{2b} is GRM1885C1H471FA01D. All impedance measurements were performed with a HP 4194A impedance/gain-phase analyzer.

-
- [1] M. Z. Hasan and C. L. Kane, *Rev. Mod. Phys.* **82**, 3045 (2010).
 [2] X.-L. Qi and S.-C. Zhang, *Rev. Mod. Phys.* **83**, 1057 (2011).
 [3] S.-Q. Shen, *Topological Insulators: Dirac Equation in Condensed Matters*, Springer Series in Solid-State Sciences, Vol. 174 (Springer-Verlag, Berlin, Heidelberg, 2012).
 [4] B. A. Bernevig, *Topological Insulators and Topological Superconductors* (Princeton University Press, Princeton, 2013).
 [5] C.-K. Chiu, J. C. Y. Teo, A. P. Schnyder, and S. Ryu, *Rev. Mod. Phys.* **88**, 035005 (2016).
 [6] A. Bansil, H. Lin, and T. Das, *Rev. Mod. Phys.* **88**, 021004 (2016).
 [7] N. P. Armitage, E. J. Mele, and A. Vishwanath, *Rev. Mod. Phys.* **90**, 015001 (2018).
 [8] W. P. Su, J. R. Schrieffer, and A. J. Heeger, *Phys. Rev. Lett.* **42**, 1698 (1979).
 [9] J. Zak, *Phys. Rev. Lett.* **62**, 2747 (1989).
 [10] Y. X. Zhao, A. P. Schnyder, and Z. D. Wang, *Phys. Rev. Lett.* **116**, 156402 (2016).
 [11] In the equations, the symmetry symbols also denote their corresponding operators (i.e., representation in the physical system).
 [12] E. Wigner, *Ann. Math.* **40**, 149 (1939).
 [13] J. Zak, *Phys. Rev.* **134**, A1602 (1964).
 [14] Y. X. Zhao, Y.-X. Huang, and S. A. Yang, *Phys. Rev. B* **102**, 161117(R) (2020).
 [15] Z. Y. Chen, Z. Zhang, S. A. Yang, and Y. X. Zhao, *Nat. Commun.* **14**, 743 (2023).
 [16] Y.-X. Huang, Z. Y. Chen, X. Feng, S. A. Yang, and Y. X. Zhao, *Phys. Rev. B* **106**, 125102 (2022).
 [17] J. Herzog-Arbeitman, Z.-D. Song, L. Elcoro, and B. A. Bernevig, *Phys. Rev. Lett.* **130**, 236601 (2023).
 [18] Y. Fang and J. Cano, *Phys. Rev. B* **107**, 245108 (2023).
 [19] H. Xue, Z. Wang, Y.-X. Huang, Z. Cheng, L. Yu, Y. X. Foo, Y. X. Zhao, S. A. Yang, and B. Zhang, *Phys. Rev. Lett.* **128**, 116802 (2022).
 [20] T. Li, J. Du, Q. Zhang, Y. Li, X. Fan, F. Zhang, and C. Qiu, *Phys. Rev. Lett.* **128**, 116803 (2022).
 [21] L. B. Shao, Q. Liu, R. Xiao, S. A. Yang, and Y. X. Zhao, *Phys. Rev. Lett.* **127**, 076401 (2021).
 [22] H. Xue, Z. Y. Chen, Z. Cheng, J. X. Dai, Y. Long, Y. X. Zhao, and B. Zhang, *Nat. Commun.* **14**, 4563 (2023).
 [23] Y. X. Zhao, C. Chen, X.-L. Sheng, and S. A. Yang, *Phys. Rev. Lett.* **126**, 196402 (2021).
 [24] Y. Meng, S. Lin, B.-j. Shi, B. Wei, L. Yang, B. Yan, Z. Zhu, X. Xi, Y. Wang, Y. Ge, S.-q. Yuan, J. Chen, G.-G. Liu, H.-x. Sun, H. Chen, Y. Yang, and Z. Gao, *Phys. Rev. Lett.* **130**, 026101 (2023).
 [25] W. B. Rui, Y. X. Zhao, and Z. D. Wang, *Phys. Rev. Lett.* **131**, 176402 (2023).
 [26] L. Shao, Z. Chen, K. Wang, S. A. Yang, and Y. Zhao, *Phys. Rev. B* **108**, 205126 (2023).
 [27] T. Li, L. Liu, Q. Zhang, and C. Qiu, *Commun. Phys.* **6**, 268 (2023).
 [28] Z. Y. Chen, S. A. Yang, and Y. X. Zhao, *Nat. Commun.* **13**, 2215 (2022).
 [29] C. Zhang, Z. Y. Chen, Z. Zhang, and Y. X. Zhao, *Phys. Rev. Lett.* **130**, 256601 (2023).
 [30] C.-A. Li, J. Sun, S.-B. Zhang, H. Guo, and B. Trauzettel, *Phys. Rev. B* **108**, 235412 (2023).
 [31] Z. Pu, H. He, W. Deng, X. Huang, L. Ye, J. Lu, M. Ke, and Z. Liu, *Phys. Rev. B* **108**, L220101 (2023).
 [32] Z. Zhu, L. Yang, J. Wu, Y. Meng, X. Xi, B. Yan, J. Chen, J. Lu, X. Huang, W. Deng *et al.*, [arXiv:2305.08450](https://arxiv.org/abs/2305.08450).
 [33] Y. Wang, C. Zhang, Z. Y. Chen, B. Liang, Y. X. Zhao, and J. Cheng, [arXiv:2305.07174](https://arxiv.org/abs/2305.07174).
 [34] Y.-L. Tao, M. Yan, M. Peng, Q. Wei, Z. Cui, S. A. Yang, G. Chen, and Y. Xu, [arXiv:2305.09174](https://arxiv.org/abs/2305.09174).
 [35] Y.-L. Tao, J.-H. Wang, and Y. Xu, [arXiv:2307.00486](https://arxiv.org/abs/2307.00486).

- [36] A. Grossi e Fonseca, S. Vaidya, T. Christensen, M. C. Rechtsman, T. L. Hughes, and M. Soljačić, [arXiv:2310.18485](#).
- [37] J. Ningyuan, C. Owens, A. Sommer, D. Schuster, and J. Simon, [Phys. Rev. X **5**, 021031 \(2015\)](#).
- [38] V. V. Albert, L. I. Glazman, and L. Jiang, [Phys. Rev. Lett. **114**, 173902 \(2015\)](#).
- [39] S. Imhof, C. Berger, F. Bayer, J. Brehm, L. W. Molenkamp, T. Kiessling, F. Schindler, C. H. Lee, M. Greiter, T. Neupert *et al.*, [Nat. Phys. **14**, 925 \(2018\)](#).
- [40] N. R. Cooper, J. Dalibard, and I. B. Spielman, [Rev. Mod. Phys. **91**, 015005 \(2019\)](#).
- [41] J. Dalibard, F. Gerbier, G. Juzeliūnas, and P. Öhberg, [Rev. Mod. Phys. **83**, 1523 \(2011\)](#).
- [42] S. Raghu and F. D. M. Haldane, [Phys. Rev. A **78**, 033834 \(2008\)](#).
- [43] T. Ozawa, H. M. Price, A. Amo, N. Goldman, M. Hafezi, L. Lu, M. C. Rechtsman, D. Schuster, J. Simon, O. Zilberberg, and I. Carusotto, [Rev. Mod. Phys. **91**, 015006 \(2019\)](#).
- [44] Z. Yang, F. Gao, X. Shi, X. Lin, Z. Gao, Y. Chong, and B. Zhang, [Phys. Rev. Lett. **114**, 114301 \(2015\)](#).
- [45] H. Xue, Y. Yang, and B. Zhang, [Nat. Rev. Mater. **7**, 974 \(2022\)](#).
- [46] C. L. Kane and T. C. Lubensky, [Nat. Phys. **10**, 39 \(2014\)](#).
- [47] G. Ma, M. Xiao, and C. T. Chan, [Nat. Rev. Phys. **1**, 281 \(2019\)](#).